# Electronic Supporting Information

## Light-driven micromotors for on-demand and local pH sensing applications

Srikanta Debata, Shivani Sahu[†], Suvendu Kumar Panda, and Dhruv Pratap Singh[*]

*Department of Physics, IIT Bhilai, Kutelabhata, Durg, Chattisgarh,491001, India.*

*[†]On M. Sc. research project from Center for Basic Sciences, PRSU, Raipur, 492010, India.*

[*]Corresponding Author: dhruv@iitbhilai.ac.in

## 1. Guide to supplementary Videos:

**Video S1:** Video shows the active swimming of micromotors in 2.5 % conc. of peroxide medium (pH ~ 5.5) under low-intensity UV light irradiation. The playback speed is 2X.

**Video S2:** Video shows the directional swimming of micromotors in the presence of an external magnetic field under low-intensity UV light irradiation. The playback speed is 4X.

**Video S3:** Video shows the swimming of micromotors in 2.5 % conc. of peroxide medium at different pH (~3, ~5.5, ~7.5, ~9) under low-intensity UV light irradiation. The playback speed is 1X.

**Video S4:** Video shows the local measurement of the pH of the medium at far and near high pH source locations using the micromotors. The pH variation in the medium was made through a syringe pump, where pH 9 solution flowed with a rate of 10 μL $min^{-1}$. The playback speed is 2X.

## 2. Supplementary figure description

### 2.1 XRD analysis:

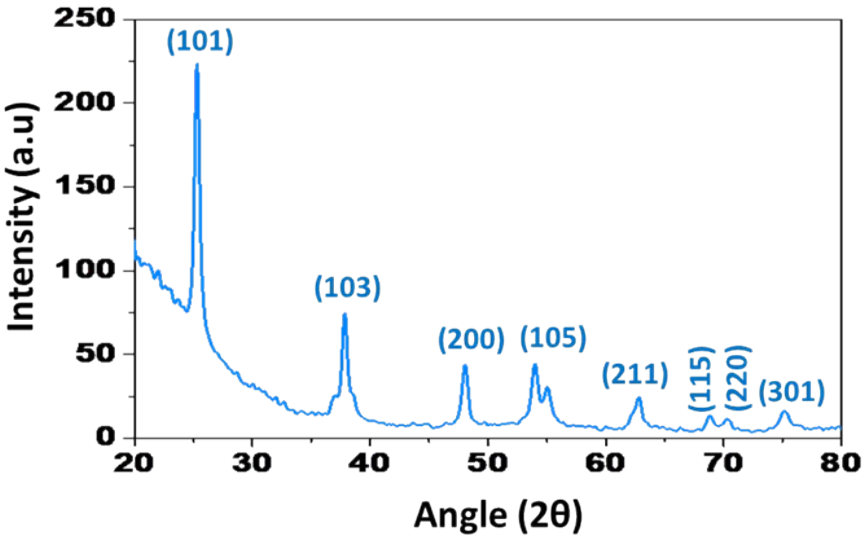


**Fig. S1** XRD analysis ensures the formation of the anatase phase of $TiO_2$.

### 2.2 SEM image of the designed micromotors:

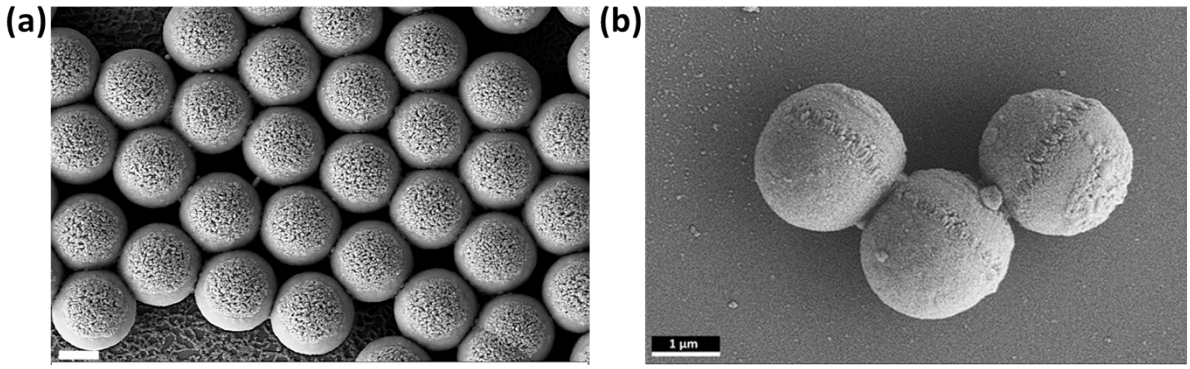


**Fig. S2** SEM image of the designed micromotors. (a) The top view of designed micromotors with closed packing on silicon wafer. (b) Randomly oriented final design of micromotors (SEM taken after drying the micromotors taken from the water solution). The scale bar represents 1 µm.

### 2.3 UV-vis absorption analysis:

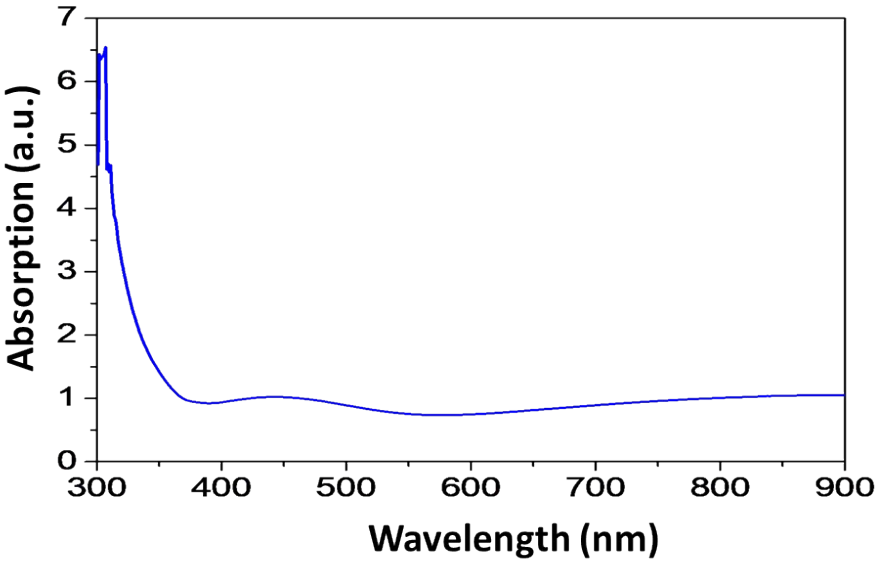


**Fig. S3** Absorption spectra of the fluorescein dye-coated micromotors.

## 2.4 Speed control under driving conditions:

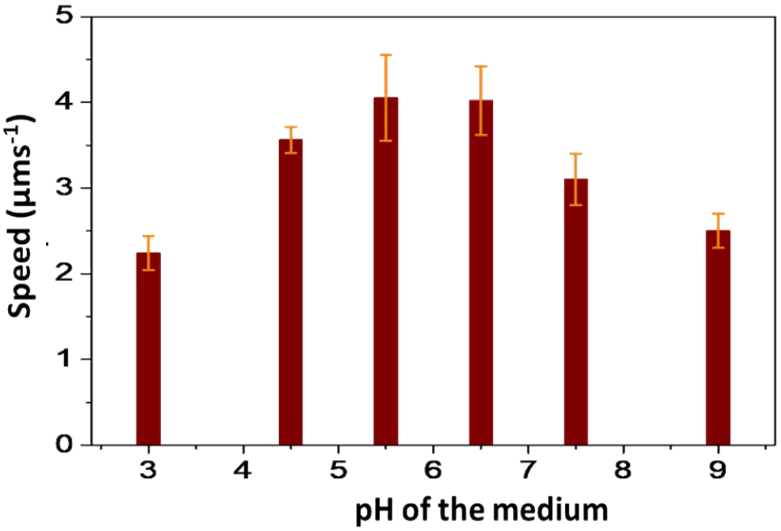


**Fig. S4** The speed of the micromotors under varying pH conditions within the 2.5% concentration of $H_2O_2$ fuel medium.

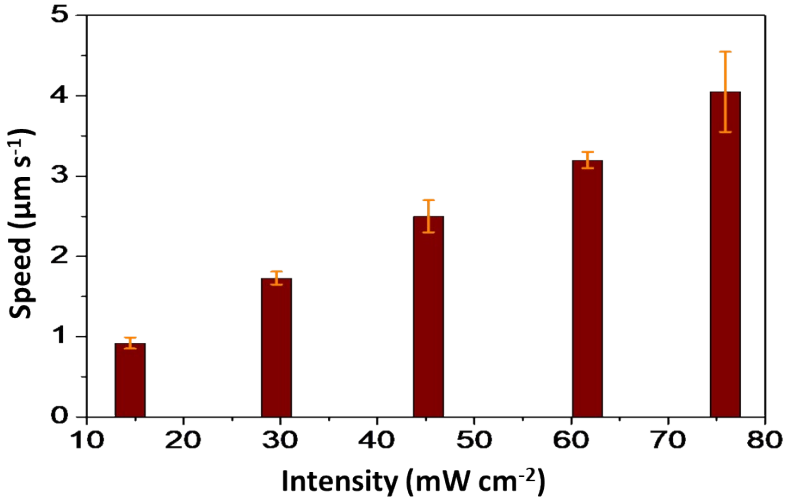


**Fig. S5** The speed of the micromotors at different intensities of the incident light.

## 2.5 Fluorescence emission spectra of fluorescein dye:

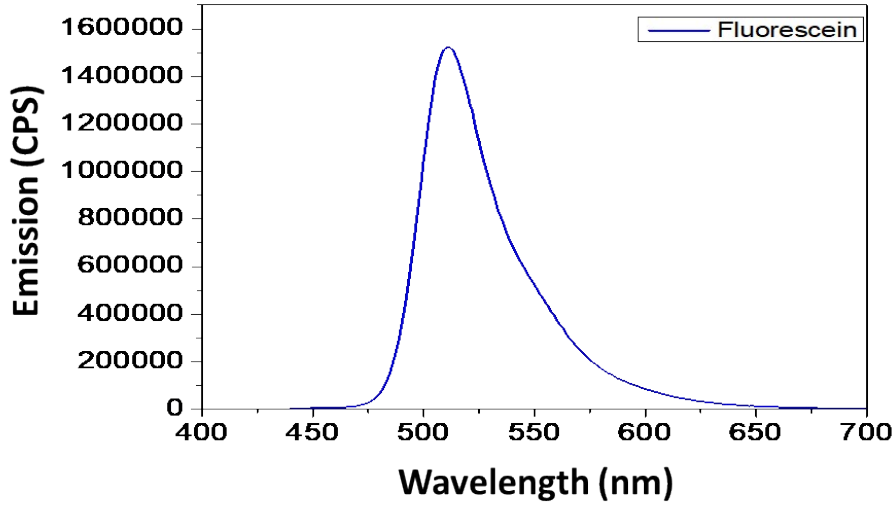


**Fig. S6** Fluorescent emission spectra show the fluorescent emission peak at the 525 nm wavelength range.

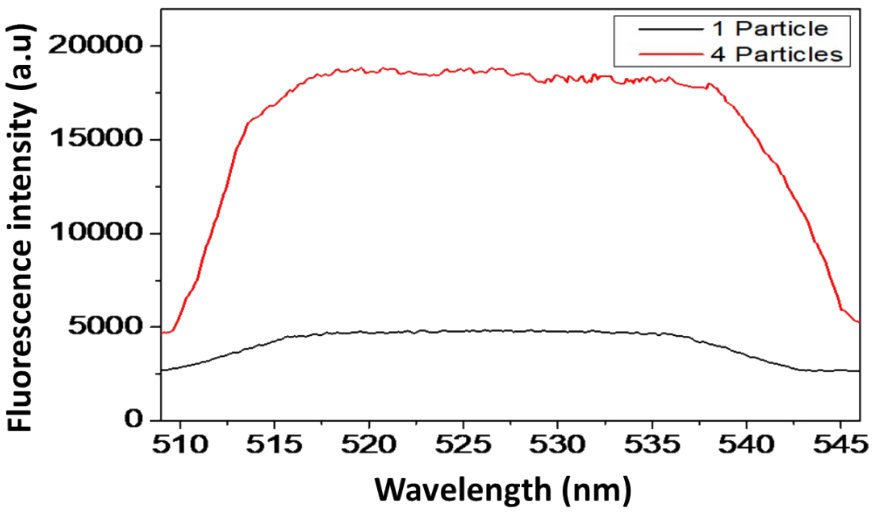


**Fig. S7**Fluorescent intensities comparison of a single particle and the group of 4 particles at a time.

## 3. Swimming mechanism of micromotors:

The propulsion mechanism can be understood through self-phoresis as shown in the schematic presented in Fig. S8. In the figure, we exclusively illustrated the role of the photocatalytic layer in the propulsion mechanism. Despite the presence of a very thin dye layer on top of the photocatalytic layer (with a thickness of 10 nm), it does not impede the photocatalytic decomposition of the surrounding fuel medium due to its extremely thin size. At this scale, nanoparticles or island structures typically form within a thin film, making a discontinuous film while leaving free space/gaps between the nanoparticles. These gaps facilitate the escape of photogenerated charge carriers from the photocatalyst to participate in the reaction.

The overall reaction mechanism can be elucidated as follows: when low-intensity UV light irradiates the $TiO_2$ surface, matching its band gap energy, electrons and holes are generated. These photogenerated electrons and holes undergo a redox reaction with the surrounding fuel medium, creating a gradient in chemical concentration. As only one-half of the micromotor participates in the reaction, a phoretic fluid flow (slip flow) around the micromotor ensues from a higher concentration region to a lower concentration region, propelling the micromotor.

Determining the precise mechanism out of the possible diffusiophoresis or electrophoresis mechanisms at this small scale is challenging (https://doi.org/10.1021/jacs.3c09223).

However, we would like to refer to some standard articles that have reported a similar propulsion mechanism with the same photocatalyst.

a. https://doi.org/10.1002/adma.201701328,
b. https://doi.org/10.1002/adfm.201706660,
c. https://doi.org/10.1002/adma.201603374,
d. https://doi.org/10.1002/asia.201900377.

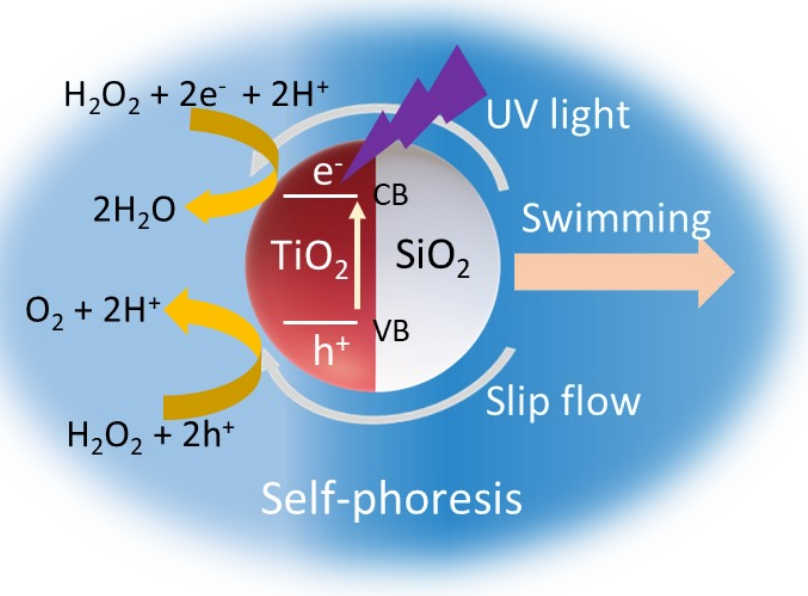


Fig. S8: Schematic represents the propulsion mechanism of the designed micromotor in peroxide fuel medium under the irradiation of UV light.

## 4. Mechanism of fluorescence intensity change with respect to pH of the medium:

Fluorescein is a complex organic fluorophore that exists in any of the four prototropic forms neutral, cation, monoanionic, and dianion depending upon the pH of the medium[1] (see Fig. S9).

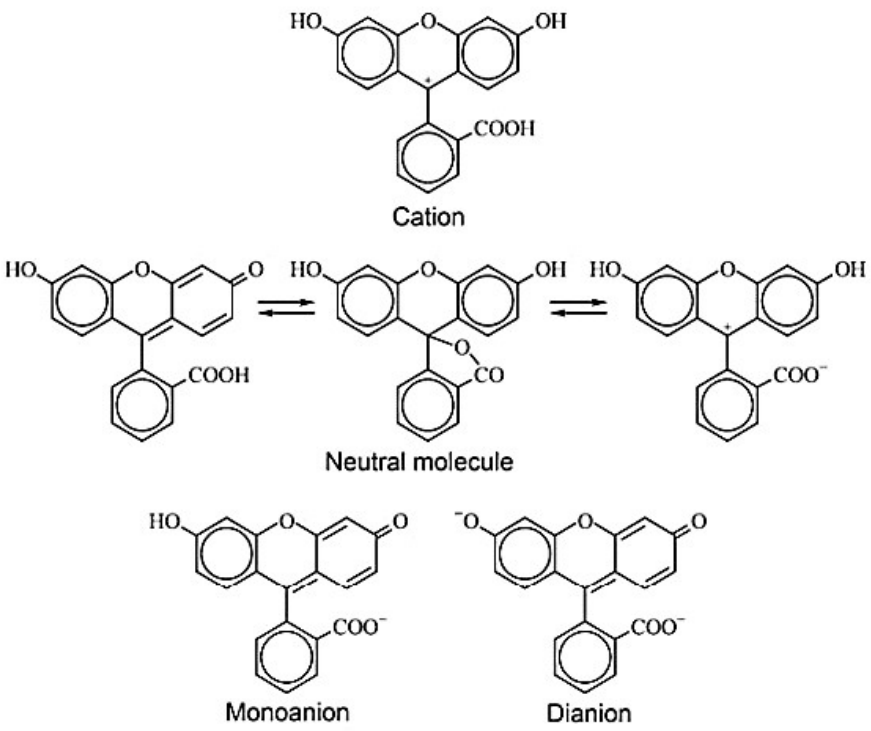


**Fig. S9:** Prototropic forms of fluorescein dye.

Out of all prototropic forms of fluorescein dye, monoanionic and dianion phases are significant in the acid-base pH media[2]. The intensity of the fluorescence signal increases with the increase in the pH of the medium as shown in Fig. 4a. The reason behind the fluorescence intensity change is OH group protonation is observed between the monoanionic and dianion phase as shown in the figure below[3] (Fig. S10).

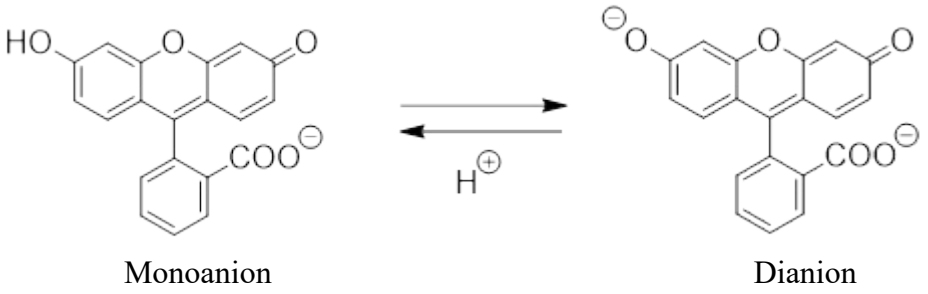


**Fig. S10:** Molecular structure and protonation at the ground state of monoanionic and dianion phases of fluorescein dye.

The geometrical configuration of both phases of fluorescein dye is very similar in the relevant pH range of our work. However, fluorescein is symmetric in the deprotonation state and antisymmetric in the protonation state of oxygen. Despite the similarity in geometrical structures, the dianion and monoanionic phases exhibit different electronic configurations, as shown by Tamulis et al. using the density functional theory[4]. The dianion molecules upon

excitation, will dissipate energy in the form of vibration and rotation until it reaches the first excitation energy state from which it will further be de-excited to its ground state by emitting photons is the most probable scenario. The forbidden transition states of dianion phases are allowed for monoanionic cases due to the low symmetry and as a result of which, the uniform distribution of energy between them will take place. Moreover, the oscillation strength of the monoanionic phase at the first excited state is smaller than the dianion phase and the energy difference between the first and second excited state is higher for the monoanion than that of the dianion. As a result of which, the quantum yield of the monoanionic phase is less than that of the dianion phase due to the larger dissipation of radiationless energy. Therefore, a monoanionic phase that exists in the acidic condition has a fluorescence intensity lower than that of the dianion phase which forms in the basicity of the medium.

## 5. Stability of micromotors under saline medium:

To validate the stability of our micromotors, we examined their performance in a real-salt medium. The propulsion speed of the micromotors remains consistent at lower salt concentrations. Our micromotors demonstrate robust stability of the fluorescence (FL) signal and efficient propulsion even in a reasonably high salt-concentration media. An experiment was conducted in a 0.2M NaCl salt medium, representing a high concentration, and our micromotors exhibited excellent stability with no significant change in the FL signal over time. Furthermore, motility performance was studied at this concentration, revealing an average motor speed of $1.75 \pm 0.2$ μm $s^{-1}$ which is slightly lower than the normal speed of the micromotors. Fig. S11 illustrates the stability of the FL signal overtime at 0.2M NaCl salt concentration, and Fig. S12 presents the tracks of the motors during swimming.

While the speed of micromotors may change in higher salt concentrations, it is challenging to pinpoint the exact mechanism of propulsion through salt testing [https://doi.org/10.1021/jacs.3c09223]. As the salt concentration increases, the agglomeration of particles or their sticking with walls/surfaces increases due to the ions-induced attraction or Vander wall forces among the particles [https://doi.org/10.1016/j.jcis.2021.10.194]. Considering that, the salt test does not provide conclusive evidence about the precise propulsion mechanism in micromotors. However, from the observed result, it is suggested that the possibility of self-electrophoresis is lower compared to the diffusion of neutral molecules.

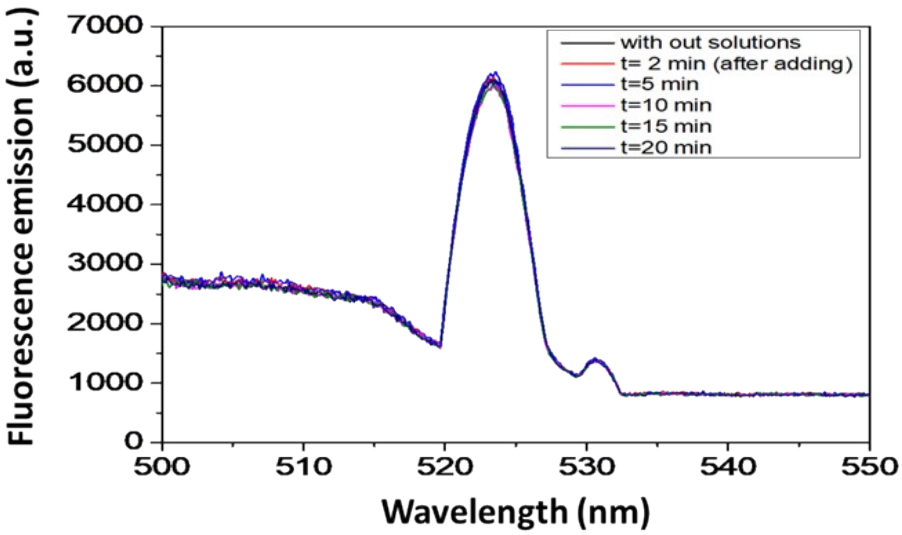


Fig. S11: Fluorescence signal of the dye-coated micromotor without adding the solutions and after adding the 0.2M concentration of aqueous NaCl solutions at different time intervals.

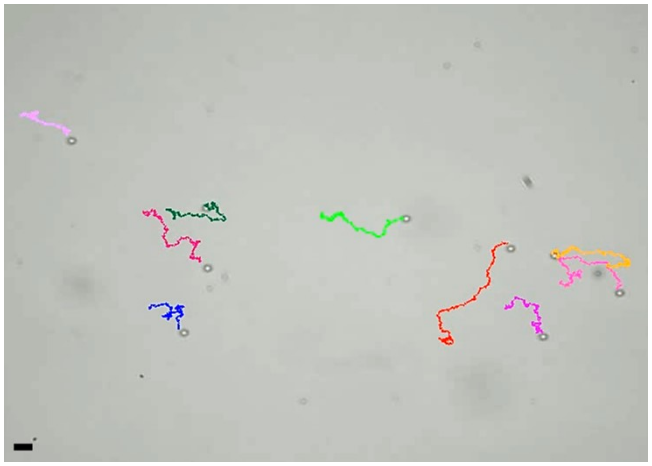

Fig. S12: Different color trajectories represent the path followed by micromotors during their active motion in the fuel medium containing 0.2 M concentration of NaCl for a time interval of 45 sec. The scale bar represents 5 µm

## References


1 N. Klonis and W. H. Sawyer, *J Fluoresc*, 1996, **6**, 147–157.

2 E. A. Slyusareva, M. A. Gerasimov, A. G. Sizykh and L. M. Gornostaev, *Russ Phys J*, 2011, **54**, 485–492.

3 J. M. Alvarez-Pez, L. Ballesteros, E. Talavera and J. Yguerabide, *J. Phys. Chem. A*, 2001, **105**, 6320–6332.

4 A. Tamulis, J. Tamuliene, M. L. Balevicius, Z. Rinkevicius and V. Tamulis, *Structural Chemistry*, 2003, **14**, 643–648.